CHARACTERIZATION OF THE SOLAR RADIATION PRESSURE PERTURBATION IN THE ECCENTRICITY VECTOR

J. Sánchez[(1)]**, M. A. Martín Serrano**[(2)]**, and R. Mackenzie**[(3)]
[(1)]*GMV at ESA/ESOC, Robert-Bosch-Str. 5, 64293 Darmstadt Germany,*
telephone: +496151902416, E-mail: javier.sanchez@esa.int
[(2)]*SCISYS GmbH at ESA/ESOC, Robert-Bosch-Straße 5, 64293 Darmstadt Germany,*
telephone: +496151902273, E-mail: miguel.angel.martin.serrano@esa.int
[(3)]*ESA/ESOC, Robert-Bosch-Straße 5, 64293 Darmstadt Germany,*
telephone: +496151902595, E-mail: ruaraidh.mackenzie@esa.int

Abstract: *Frozen eccentricity orbits are common in Earth Observation missions flying in Low Earth Orbit (LEO) since these missions typically require altitude control. The frozen eccentricity concept is based on the existence of values for the argument of perigee and the eccentricity for which the Earth's potential long-periodic perturbation nullifies. These are the so-called frozen eccentricity values. In the vicinity of these stability points the eccentricity vector describes a rotation at nearly constant angular velocity; this known behaviour is the basis of most passive eccentricity control strategies. When other perturbations are considered, the evolution of the eccentricity vector adopts a more complex pattern. In particular, the disturbing effect of the Solar Radiation Pressure (SRP) is clearly visible when the eccentricity vector is close to the frozen value. Commonly used eccentricity control algorithms determine iteratively corrections to the eccentricity vector based on full-perturbations-model numerical integrations. However, the analytical derivation of the eccentricity vector motion taking into account the Earth's potential and the SRP perturbations is of high advantage in the design of efficient eccentricity control strategies. This paper presents such an analytical approach to the eccentricity control problem, analysing the SRP perturbation effect with and without eclipse conditions. Applications of this result to the eccentricity control problem for ESA missions Sentinel-1 and 2 are provided.*

Keywords: *Eccentricity, Solar Radiation Pressure, Orbit Control, Altitude Control.*

1. Introduction

Most Earth Observation payloads are designed to perform regular observations of the same areas on the Earth's surface. Applying comparative techniques to the acquired data is often possible only when altitude variations between data takes are below a required threshold. This requirement drives the selection of the mission's operational orbit as well as the design of the operational orbit maintenance strategy. The selection of frozen eccentricity orbits is suitable to keep control on the long term evolution of the eccentricity vector caused by the Earth's potential perturbation and by doing that controlling changes in altitude. Frozen eccentricity orbits have a mean argument of perigee close to 90 degrees combined with an eccentricity value that reduces the effect of the Earth's potential perturbation to zero. When the eccentricity vector is in the vicinity of this point, its long-periodic variation describes a rotation at constant angular velocity around this stability point [1], [2].

As already mentioned, the frozen eccentricity concept relies on the perturbation from the Earth's potential, which in LEO is the main one. However, when other perturbations are considered, the

evolution of the eccentricity vector adopts a more complex pattern. In particular, the disturbing effect of the Solar Radiation Pressure (SRP) is clearly visible when the eccentricity vector is close to the frozen value. Neglecting higher order terms it can be demonstrated that the perturbation in the eccentricity vector due to the SRP can be approximated by a seasonal-dependent constant drift in the e_x, e_y plane. The seasonal dependency is given by the orientation of the Sun direction with respect to the orbital plane. Orbit control strategies commonly make use of full-force-model numerical integrations to correct regularly the eccentricity vector during the operational phase. These corrections make use of the selected frozen eccentricity to passively achieve the eccentricity control as part of the maintenance of the semi-major axis. Nonetheless, the analytical derivation of the eccentricity vector motion taking into account the Earth's potential and the SRP perturbations is of high advantage in the design of efficient eccentricity control strategies, specially when a full passive eccentricity control is not possible due to strict constraints in altitude variations.

This paper is concerned with such an analytical approach. In section 2 the effect of the SRP force on the eccentricity vector is modelled as the effect of a constant force on a Keplerian orbit. Section 3 considers the known problem of the Earth's potential perturbation in the eccentricity vector and its motion in the vicinity of the frozen eccentricity. The combined effect of both perturbations is presented in section 4 and applications to the ESA Copernicus missions Sentinel-1 and Sentinel-2 are given in section 5.

In the notation used throughout this paper vectors are represented as $\vec{a}$ in the equations or using **bold** letters in the text.

2. Effect of the SRP on the eccentricity vector

This section is dedicated to model the perturbation of the SRP in the eccentricity vector. In the analysis presented hereinafter the following is assumed:

- The force exerted by the SRP on the main body can be neglected with respect to that on the orbiting body. This is true since the ratio Surface/Mass is usually several orders of magnitude higher for the latter.
- The seasonal change in magnitude and direction of the SRP force with respect to a reference frame fixed to the orbit is much slower than the orbital period.
- The SRP is a constant force acting all along the orbit in a direction defined from the Sun to the Earth.

Based on these assumptions the SRP force (per unit mass) can be expressed as a constant vector, as shown in Eq. 1, by its Cartesian components in the frame {$\mathbf{u_x}$, $\mathbf{u_y}$, $\mathbf{u_z}$} fixed to the orbit, with $\mathbf{u_z}$ in the direction of the angular momentum, $\mathbf{u_x}$ in the direction of the eccentricity vector, and $\mathbf{u_y}$ completing a right-handed frame. The effect of the SRP shall be computed as a perturbation to a Keplerian orbit, assumed as zeroth order solution. Therefore the {$\mathbf{u_x}$, $\mathbf{u_y}$, $\mathbf{u_z}$} can be considered fixed. In the same frame, the position and velocity vectors can be expressed as a function of the true anomaly as shown in Eq. 2 and 3.

$$\vec{\gamma} = \gamma_x \vec{u}_x + \gamma_y \vec{u}_y + \gamma_z \vec{u}_z \tag{1}$$

$$\vec{r} = r\cos f\vec{u}_x + r\sin f\vec{u}_y \tag{2}$$

$$\dot{\vec{r}} = -\frac{\mu}{h}\sin f\vec{u}_x + \frac{\mu}{h}(e+\cos f)\vec{u}_y \tag{3}$$

Following the Gauss form of the variational equations, the change in angular momentum and eccentricity vector caused by a small perturbing acceleration can be expressed as shown in Eq. 6 and 8.

$$\ddot{\vec{r}} = -\frac{\mu}{r^3}\vec{r} + \vec{\gamma} \tag{4}$$

$$\vec{h} = \vec{r} \times \dot{\vec{r}} \tag{5}$$

$$\dot{\vec{h}} = \vec{r} \times \vec{\gamma} \tag{6}$$

$$\vec{e} = \frac{\dot{\vec{r}} \times \vec{h}}{\mu} - \frac{\vec{r}}{r} \tag{7}$$

$$\dot{\vec{e}} = \frac{\dot{\vec{r}} \times \dot{\vec{h}}}{\mu} - \frac{\mu}{r^3}\vec{r} \times \frac{\vec{h}}{\mu} + \frac{\vec{\gamma} \times \vec{h}}{\mu} + \frac{\vec{r} \times \vec{h}}{r^3} = \frac{\dot{\vec{r}} \times \dot{\vec{h}}}{\mu} + \frac{\vec{\gamma} \times \vec{h}}{\mu} \tag{8}$$

Eq. 10 and 11 show the effect of the perturbing acceleration component perpendicular to the orbital plane. It is observed that this component of the perturbation makes the eccentricity and angular momentum move as a rigid body. Additionally, an order of magnitude of the eccentricity drift can be extracted from Eq. 10, which is smaller by a factor of e than the one induced by a coplanar acceleration, as it will be shown later.

$$\dot{\vec{e}} = \frac{\dot{\vec{r}} \times (\vec{r} \times \gamma_z\vec{u}_z)}{\mu} + \frac{\gamma_z\vec{u}_z \times \vec{h}}{\mu} = \frac{(\dot{\vec{r}} \cdot \gamma_z\vec{u}_z)\vec{r} - (\vec{r} \cdot \dot{\vec{r}})\gamma_z\vec{u}_z}{\mu} = -\frac{\gamma_z}{h\mu}(\vec{r} \cdot \dot{\vec{r}})\vec{h} \tag{9}$$

$$\dot{\vec{e}} = \frac{\gamma_z}{h\mu}(\vec{r} \times (\dot{\vec{r}} \times \vec{h})) = \left(\frac{\gamma_z\vec{r}}{h}\right) \times \left(\frac{\dot{\vec{r}} \times \vec{h}}{\mu} - \frac{\vec{r}}{r}\right) = \left(\frac{\gamma_z\vec{r}}{h}\right) \times \vec{e} \tag{10}$$

$$\dot{\vec{h}} = \left(\frac{\gamma_z\vec{r}}{h}\right) \times \vec{h} \tag{11}$$

The change in the eccentricity vector due to the component of γ contained in the orbital plane can be derived from Eq. 8 by making use of Eq. 2, 3, 5 and 6. This results in the eccentricity vector variation expressed in Eq. 12 and 13.

$$\dot{e}_x = \frac{1}{h}\left[(e + \cos f)(\gamma_y r \cos f - \gamma_x r \sin f) + \gamma_y p\right] \tag{12}$$

$$\dot{e}_y = \frac{1}{h}\left[\sin f(\gamma_y r \cos f - \gamma_x r \sin f) - \gamma_x p\right] \tag{13}$$

The eccentricity change given in the previous equations can be averaged over an orbit revolution. If no eclipse along the orbit is assumed (i.e. the effect of the perturbing acceleration is active all along the orbit) and neglecting terms of the order of $O(pe^2)$ the average eccentricity vector change is given by Eq. 17 and 18. Notice that the resulting eccentricity variation is perpendicular to the perturbing acceleration by a $\pi/2$ negative rotation.

$$r = p(1 - e \cos f) + O(pe^2) \tag{14}$$

$$\tilde{e}_x = \frac{1}{2\pi}\frac{1}{h}\int_0^{2\pi} \ [\ \gamma_y ep \cos f - \gamma_y e^2 p \cos^2 f - \gamma_x ep \sin f + \gamma_x e^2 p \sin f \cos f +$$
$$+ \gamma_y p \cos^2 f - \gamma_y ep \cos f \cos^2 f - \gamma_x p \sin f \cos f + \gamma_x ep \sin f \cos^2 f + \gamma_y p]df \tag{15}$$

$$\tilde{e}_y = \frac{1}{2\pi}\frac{1}{h}\int_0^{2\pi} \ [\ \gamma_y p \sin f \cos f - \gamma_y ep \sin f \cos^2 f - \gamma_x p \sin^2 f +$$
$$+ \gamma_x ep \sin^2 f \cos f - \gamma_x p]df \tag{16}$$

$$\tilde{e}_x \cong \frac{1}{2\pi}\frac{1}{h}\int_0^{2\pi} \ [\ \gamma_y p \cos^2 f - \gamma_y ep \cos^2 f + \gamma_y p]df = \gamma_y \frac{3}{2}\frac{p}{h} \tag{17}$$

$$\tilde{e}_y \cong \frac{1}{2\pi}\frac{1}{h}\int_0^{2\pi} \ [-\gamma_x p \sin^2 f - \gamma_x p]df = -\gamma_x \frac{3}{2}\frac{p}{h} \tag{18}$$

Eclipse conditions can be included in this formulation by adding a correction to the results derived in Eq. 17 and 18. In order to simplify the process, terms of the order of $O(pe)$ have been neglected. This assumes circular orbits, which is the main focus of this work. Nevertheless, if the results are to be applied to eccentric orbits, the terms of the order of $O(pe)$ can be easily added following an analogous process. The eclipse correction term is obtained by integrating the right hand side of Eq. 15 and 16, with opposite sign, between the limits of the eclipse. Let θ_1 and θ_2 be respectively the true anomalies at the eclipse start and end. Then, the correction term is given by Eq. 19 and the average eccentricity vector variation takes the form shown in Eq. 20. Note that the correction term is also in the direction of a $\pi/2$ rotation negative rotation with respect to the direction of the coplanar component of the perturbing acceleration. As expected, the correction due to the eclipse depends on the difference $\theta_2 - \theta_1$, i.e. the eclipse length, and vanishes when this difference is zero.

$$\tilde{\tilde{e}}_{corr} \cong \frac{1}{2\pi} \frac{p}{h} \begin{bmatrix} \int_{\theta 1}^{\theta 2} \sin f \cos f df & -\int_{\theta 1}^{\theta 2} (1+\cos^2 f) df \\ \int_{\theta 1}^{\theta 2} (1+\sin^2 f) df & -\int_{\theta 1}^{\theta 2} \sin f \cos f df \end{bmatrix} \begin{bmatrix} \gamma_x \\ \gamma_y \end{bmatrix} \qquad (19)$$

$$\tilde{\tilde{e}} \cong \frac{3}{2} \frac{p}{h} \left[1 - \frac{\theta_2 - \theta_1}{2\pi} + \frac{1}{3} \frac{\sin(\theta_2 - \theta_1)}{2\pi} \right] \begin{pmatrix} 0 & 1 \\ -1 & 0 \end{pmatrix} \bar{\gamma} \qquad (20)$$

3. Earth's potential perturbation in the eccentricity: The Frozen Eccentricity

This section summarizes briefly the well known mathematical results behind the frozen eccentricity principle and describes the generation of frozen eccentricity reference orbits for Earth Observation missions.

The main perturbing force of the eccentricity vector in LEO is the Earth's potential, in particular the Zonal Harmonics J_2 and J_3. From Vallado [1] the long-term variations in the eccentricity and argument of perigee are given in Eq. 21 and 22.

$$\dot{e} = \frac{-3nJ_3 R_\oplus^3 \sin i}{2p^2 a} \left(1 - \frac{5}{4} \sin^2 i \right) \cos \omega \qquad (21)$$

$$\dot{\omega} = \frac{3nJ_2 R_\oplus^2}{p^2} \left(1 - \frac{5}{4} \sin^2 i \right) \left[1 + \frac{J_3 R_\oplus}{2J_2 p} \left(\frac{\sin^2 i - e \cos^2 i}{\sin i} \right) \frac{\sin \omega}{e} \right] \qquad (22)$$

It can be seen that $\dot{\omega}$ nullifies at the critical inclination i_w, or when the term in square brackets is zero. By fixing values for a and i, which are normally imposed by other mission requirements, a relation between e and ω can be found, which makes the rate in argument of perigee zero. On the other hand, the rate in eccentricity is nullified for equatorial orbits and orbits at the critical inclination ($i=0$ or $i=i_w$), or if the argument of perigee 90 or 270 degrees. Since most Earth Observation missions operate in polar orbits the value of the frozen eccentricity results in:

$$e_0 = -\frac{J_3 R_\oplus}{2J_2 p} \left(\frac{\sin^2 i - e \cos^2 i}{\sin i} \right) \sin \omega \qquad (23)$$

$$\omega = 90 \text{ deg} \qquad (24)$$

By linearizing the motion of the eccentricity vector given by Eq. 21 and 22 in the vicinity of its frozen value it can be demonstrated that it describes a rotation about that point. The angular rotation of this motion is derived in M. Rosengren [2] and is given in Eq. 25 and 26, and it depends on the orbit semi-major axis and inclination. Figure 1 depicts the value of the rotational period as a function of the semi-major axis, assuming Sun-synchronous relation between a and i.

$$\Omega_{FRZ} = \frac{A}{e_0} \qquad (25)$$

$$A = -\frac{3nJ_3R_\oplus^3 \sin i}{2a^3}\left(1 - \frac{5}{4}\sin^2 i\right) \qquad (26)$$
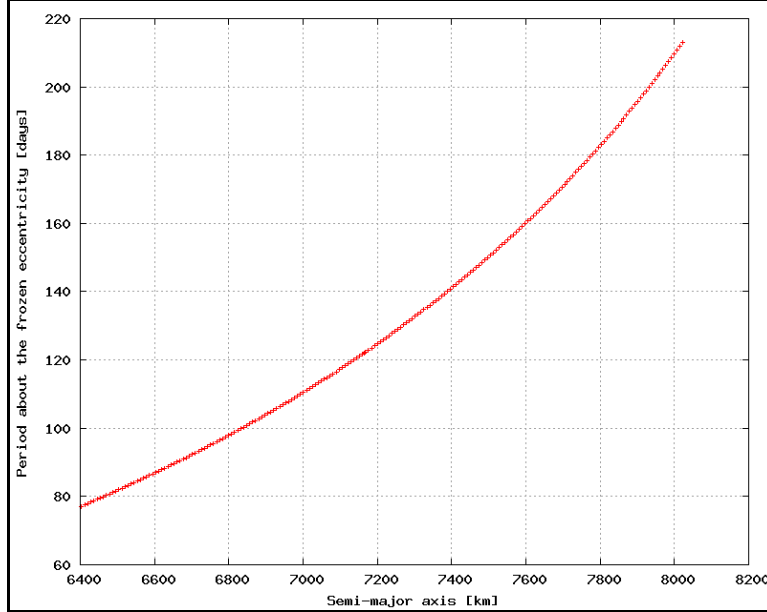

Figure 1: Rotational period around the frozen eccentricity

3.1 Frozen eccentricity reference orbits

The results on the frozen eccentricity presented above have been derived considering the effect of the J_2 and J_3 zonal harmonics. Earth's potential harmonics of higher degree and order have an influence on the precise value of the frozen eccentricity as well, leading to slightly different positions than the one given by Eq. 23 and 24. In practice, the computation can be done numerically using precise models of the Earth's potential following different approaches. M. Ronsengren [2] suggests an iterative algorithm to achieve frozen eccentricity, which is based on the assumption that in a first approximation the eccentricity vector moves as described above with the J_2 and J_3 harmonics plus a perturbing term. For missions with a ground-track repeat pattern the method that is currently used in ESOC FD is embedded in the generation of the missions' reference orbit that is used for orbit control purposes. The reference orbit is created with a propagation that only includes a detailed model of the Earth's potential. The critical point for the eccentricity is found by running an optimization in which the osculating eccentricity is constrained to be the same at the start and at end of the repeat cycle. Notice that the cycle start and end are at the same position in an Earth-Fixed reference frame. Since the length of the repeat cycle is much shorter than the rotation period about the frozen eccentricity (See Eq. 25) the optimization converges to an orbit with no long-periodic variations in the eccentricity vector. By controlling the spacecraft orbit close to this reference the short-periodic eccentricity variations are nearly the same as those of the reference orbit. That is, they are not visible when computing the relative osculating eccentricity vector with respect to the reference at correlative points in the

repeat cycle (nearly the same Earth-Fixed position). On the other hand, the osculating eccentricity vector relative to the reference is subject to the long-periodic variations undergone by the analysed orbit, which are treated in this paper.
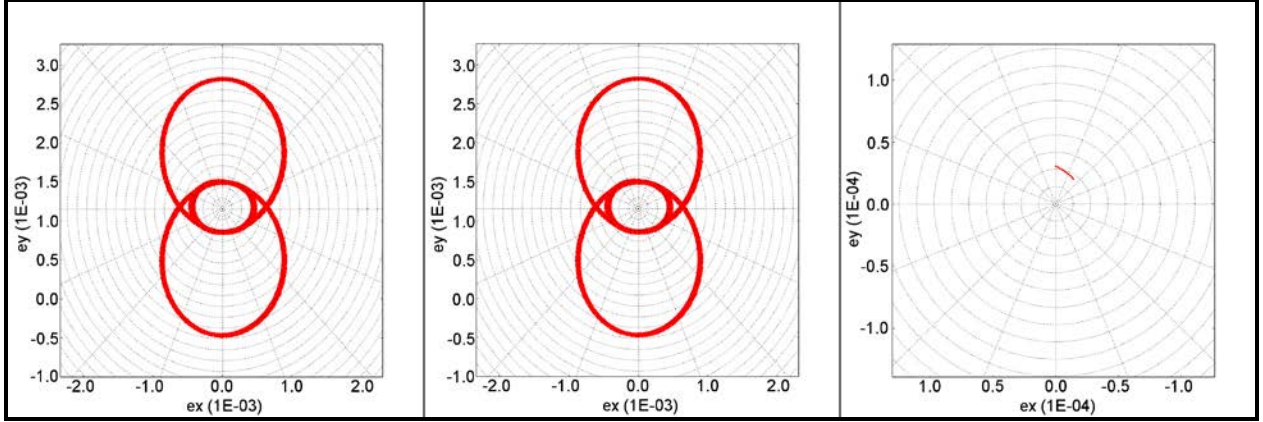
Figure 2: Osculating eccentricity vector of a reference orbit (left), an orbit following the reference (centre) and relative (right)

4. Combined effect of the Earth's potential and the SRP perturbations in the eccentricity vector

In sections 2 and 3 the eccentricity vector variation has been characterized due to both, the SRP and the Earth's potential perturbations respectively. The former induces an eccentricity drift given by Eq. 20, which is perpendicular to the projection of the SRP force onto the orbital plane. On the other hand, the study of the Earth's potential perturbation predicts the existence of a stability point, the frozen eccentricity, and the motion in the vicinity of this point can be modeled as a rotation at constant angular velocity. This section tackles the combined effect on the eccentricity vector of both perturbations.

Let $\{\mathbf{i}, \mathbf{j}, \mathbf{k}\}$ be an orthonormal base, with $\mathbf{i}$ in the direction of the line of nodes, $\mathbf{k}$ in the direction of the angular momentum and $\mathbf{j}$ completing a right handed frame. In this reference the eccentricity can be expressed by means of its (e_x, e_y) components in the $\{\mathbf{i}, \mathbf{j}\}$ space. Let $\mathbf{r}$ be the position of an arbitrary eccentricity value with respect to the frozen eccentricity (e_{0x}, e_{0y}), let $\mathit{\Omega}$ be the angular velocity of the eccentricity due to the Earth's potential perturbation about the frozen eccentricity, and let $\mathbf{v_{SRP}}$ be the eccentricity drift induced by the SRP perturbation. The combined effect can be expressed by Eq. 30, which is a system of two ordinary differential equations. It can be integrated taking into account the dependency of $\mathbf{v_{SRP}}$ with respect to the SRP force, which is a function of time (notice the seasonal position changes of the Sun with respect to the $\{\mathbf{i}, \mathbf{j}, \mathbf{k}\}$ frame). However, a qualitative analysis of this equation yields interesting results.

$$\vec{r} = \vec{e} - \vec{e}_0 \tag{27}$$

$$\vec{\Omega} = \Omega_{FRZ}\vec{k} \tag{28}$$

7

$$\vec{v}_{SRP} = \vec{v}_{SRP}(\vec{\gamma}_{SRP}) \tag{29}$$

$$\dot{\vec{r}} = \vec{\Omega} \times \vec{r} + \vec{v}_{SRP} \tag{30}$$

Equation 30 shows that the eccentricity moves within the {**i**, **j**} plane, and that the field of velocities is as that of a rigid body. Therefore, very powerful results from plane motion kinematics can be used in its study, in particular the concept of Instant Centre of Rotation (ICR). In the field of velocities defined by Eq. 30 a point with null velocity exists, the position of that point is given by solving the right-hand side of Eq. 30 equal to **0.** Let ρ be position of an arbitrary eccentricity value with respect to the ICR. The motion of the eccentricity vector with respect to the ICR is given by Eq. 33, which represents a rotation about the ICR with an angular velocity equal to Ω, which is that of the problem with just the Earth's potential perturbation.

$$\vec{r}_{ICR} = \frac{\vec{\Omega} \times \vec{v}_{SRP}}{\Omega^2} \tag{31}$$

$$\vec{\rho} = \vec{r} - \vec{r}_{ICR} \tag{32}$$

$$\dot{\vec{r}} = \vec{\Omega} \times \left(\vec{\rho} + \frac{\vec{\Omega} \times \vec{v}_{SRP}}{\Omega^2} \right) + \vec{v}_{SRP} = \vec{\Omega} \times \vec{\rho} - \vec{v}_{SRP} + \vec{v}_{SRP} = \vec{\Omega} \times \vec{\rho} \tag{33}$$

The ICR is not a static point, its motion is given by Eq. 31. Given a model for γ the vector $\mathbf{v}_{SRP}$ can be derived from Eq. 20 and the position of the ICR can be computed at any time. In general, the trajectory of the ICR varies from mission to mission and is strongly dependent on the orientation of the orbital plane. Understanding the motion of the ICR for a given mission enables the design of efficient eccentricity control strategies.

5. Application Examples

This section provides examples of the theory that has been presented so far. Two Sun-synchronous spacecraft with different orbital plane orientations have been selected. The computations of the SRP force have been done using the IERS model [3]. All eccentricity plots shown in this section represent eccentricity vectors with respect to their reference orbits.
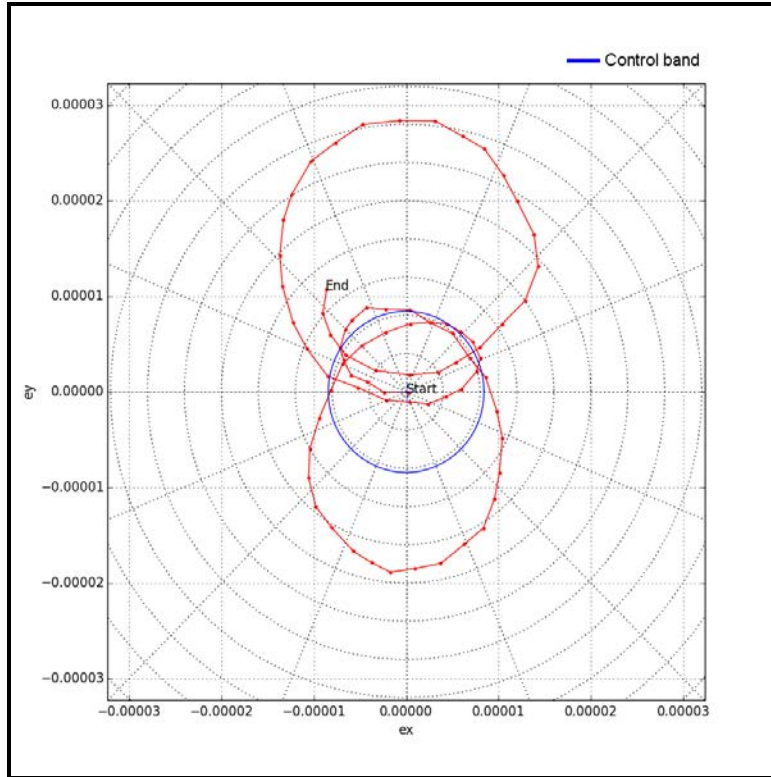
5.1. Sentinel-1 mission

Due to its tight orbit control requirements Sentinel-1 serves as a good application example, as a mission where strict eccentricity control is required. The spacecraft is controlled following a Sun-synchronous dusk-dawn orbit (see Tab. 1). The eccentricity vector is kept within 8.427E-6 units with respect to the reference orbit and Orbit Control Manoeuvres (OCM) are executed on a weekly basis. Typically the sizes span from 1 to 10 mm/s in delta-v (in-plane). Further details on the Sentinel-1 orbit control can be found in M. A. Martin Serrano [4].
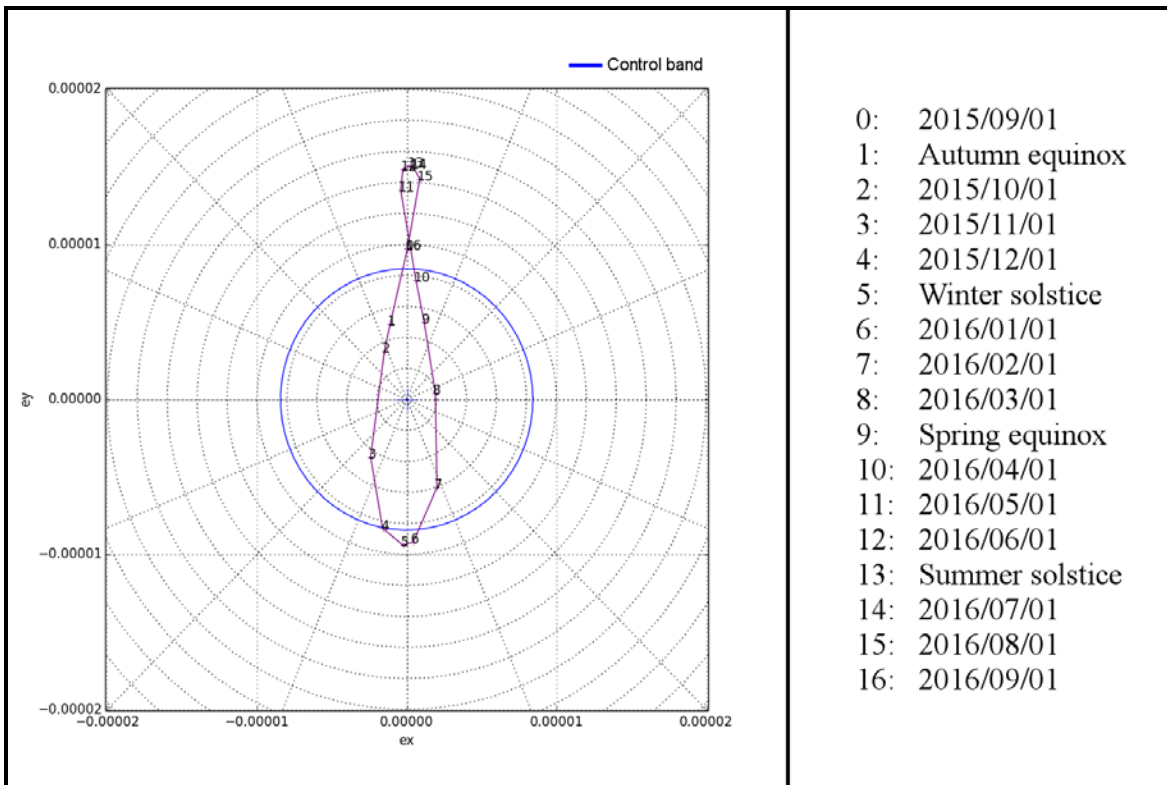
Table 1: Sentinel-1 figures

Local Time of Descending Node (Sun-synchronous)	6:00 h
Repeat ground-track pattern	175 orbits in 12 days
SRP coefficient	1.3
SRP reference surface	38 m^2
Spacecraft mass	2148 kg
Rotation period about the frozen eccentricity	115.20 days
Eclipse duration	0 to 1135 s

In spite of the dusk-dawn orientation, which minimizes the size of the SRP force projection onto the orbital plane, the relatively large reflectance area and the strict control requirements pose a challenge for the eccentricity control. Figure 3 depicts for a time span of one year the behaviour of an orbit where the eccentricity vector has not been actively controlled. The trajectory is the result of the SRP and Earth's potential perturbations together. The positions of the ICR have been represented in Fig. 4 in intervals of one month, plus both Equinoxes and Solstices. The motion of the ICR suggests an eccentricity control strategy close to the upper part of the control area during the Summer Solstice period, targeting eccentricity changes towards the positive e_x axis, as seen in Fig. 5, to compensate its natural evolution. The eccentricity vector is kept as close as possible to the upper threshold in order to reduce the drift, choosing a control path compatible with the one-week orbit control cycles. As soon as the ICR returns into the control area after the Summer Solstice period (Fig. 6), eccentricity changes will be aimed at following it down on its way to the Winter Solstice position. The Winter Solstice position is not as critical as the one in Summer due to its proximity to the control threshold. After the Winter Solstice period, the ICR will be followed up towards its position at the Summer Solstice repeating the process again.

Figure 3: Uncontrolled Sentinel-1 eccentricity vector - 1 year

0:	2015/09/01
1:	Autumn equinox
2:	2015/10/01
3:	2015/11/01
4:	2015/12/01
5:	Winter solstice
6:	2016/01/01
7:	2016/02/01
8:	2016/03/01
9:	Spring equinox
10:	2016/04/01
11:	2016/05/01
12:	2016/06/01
13:	Summer solstice
14:	2016/07/01
15:	2016/08/01
16:	2016/09/01

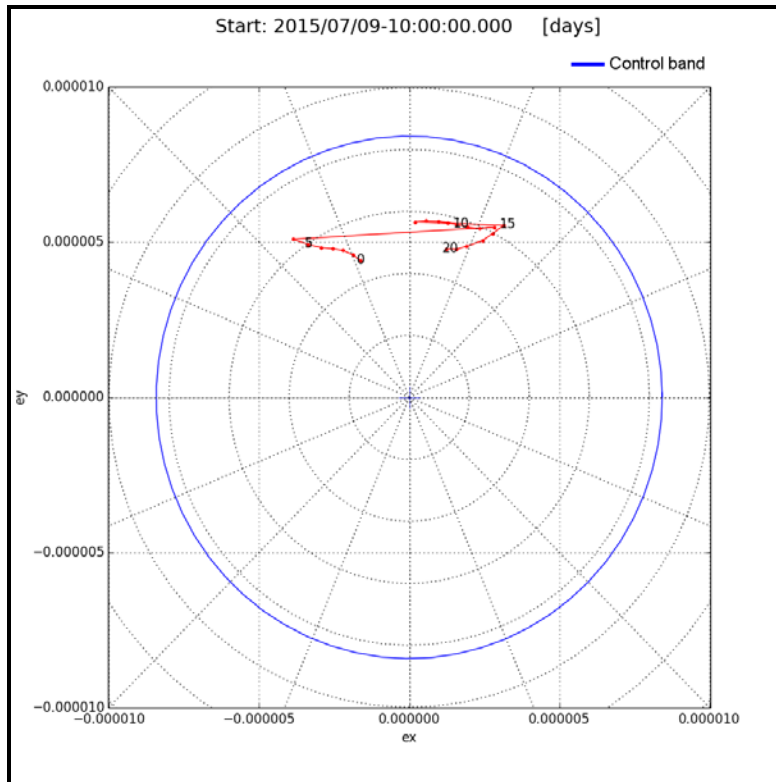**Figure 4: ICR positions for Sentinel-1**

10

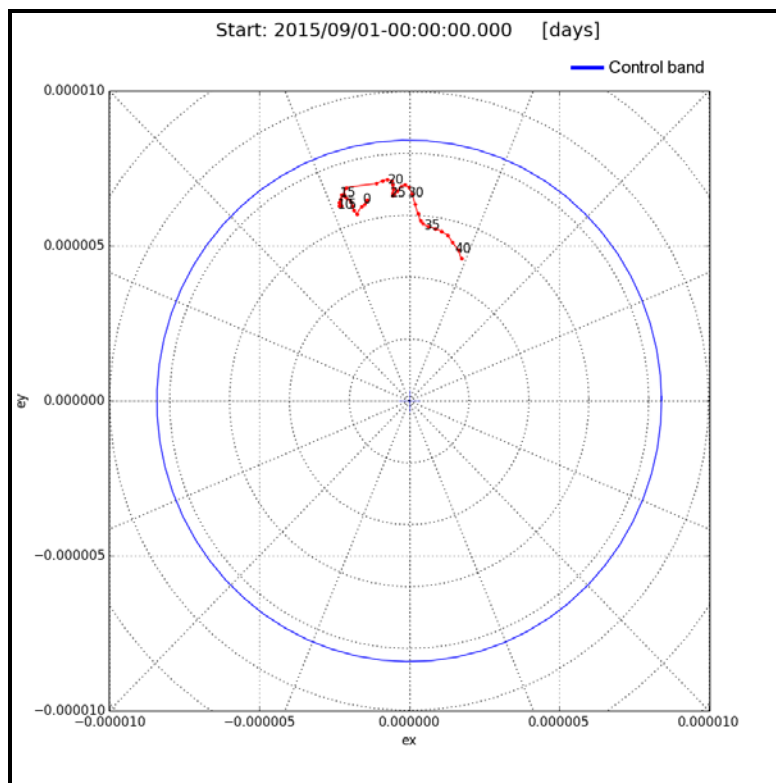**Figure 5: Sentinel-1 eccentricity vector in routine during Summer Solstice**

Figure 6: Sentinel-1 eccentricity vector in routine after Summer Solstice

5.2. Sentinel-2 mission

The tolerance in altitude variations for the Sentinel-2 mission is wider than for Sentinel-1. In this case the eccentricity vector has to be kept within 5.56E-5 units with respect to the reference orbit. However, the control is affected by limitations in the possible locations of OCMs, which is constrained to a range of arguments of latitude approximately 180 degrees in size (from 236.8 deg to 53.7 deg). This constrains the directions in which eccentricity variations can be applied to a semi-plane in the (e_x, e_y) space. OCMs are executed after periods of 30 days or longer, depending on the solar activity. Figure 7 depicts the motion of the eccentricity vector with respect to the reference orbit, where the eccentricity vector of the analysed orbit has not been controlled. Notice that the trajectory described by the eccentricity vector is almost closed, which is possible since the rotational period is a divisor of one year. The positions of the ICR have been depicted in Fig. 8 in steps of months plus both Equinoxes and Solstices. The control of the eccentricity vector in routine is done close to the ICR as it is shown in Fig. 9. OCMs are planned such that the distance to the ICR is reduced, if this cannot be done due to the constraints on the manoeuvre locations, either a double manoeuvre (no eccentricity change) or a single manoeuvre with a convenient change in phase around the ICR can be executed.

Table 2: Sentinel-2 figures

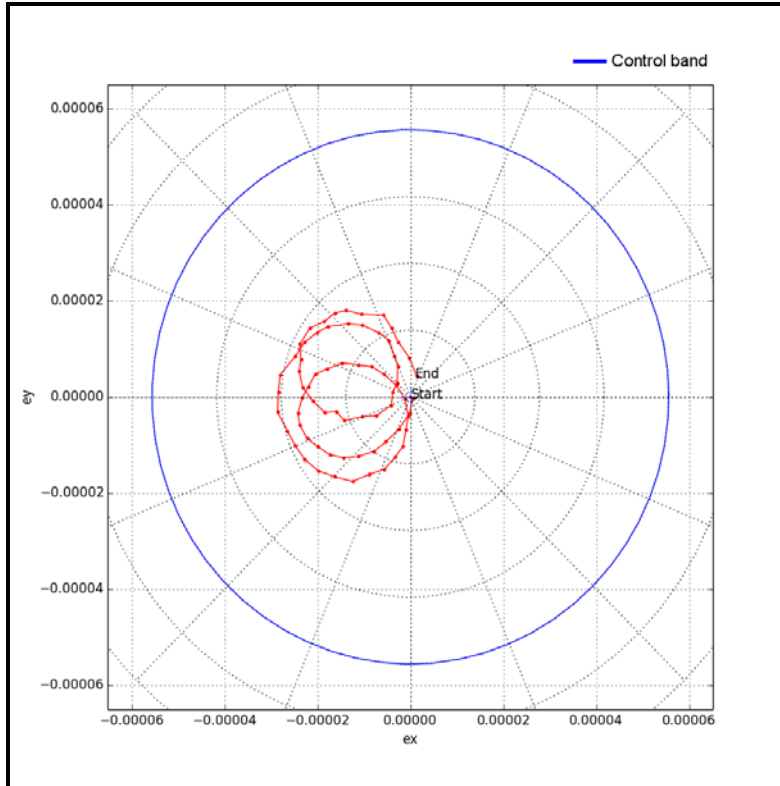|	
Local Time of Descending Node (Sun-synchronous)	10:30 h
Repeat ground-track pattern	143 orbits in 10 days
SRP coefficient	1.3
SRP reference surface	12 m^2
Spacecraft mass	1150 kg
Rotation period about the frozen eccentricity	122.38 days
Eclipse duration	2040 s

Figure 7: Uncontrolled Sentinel-2 eccentricity vector - 1 year

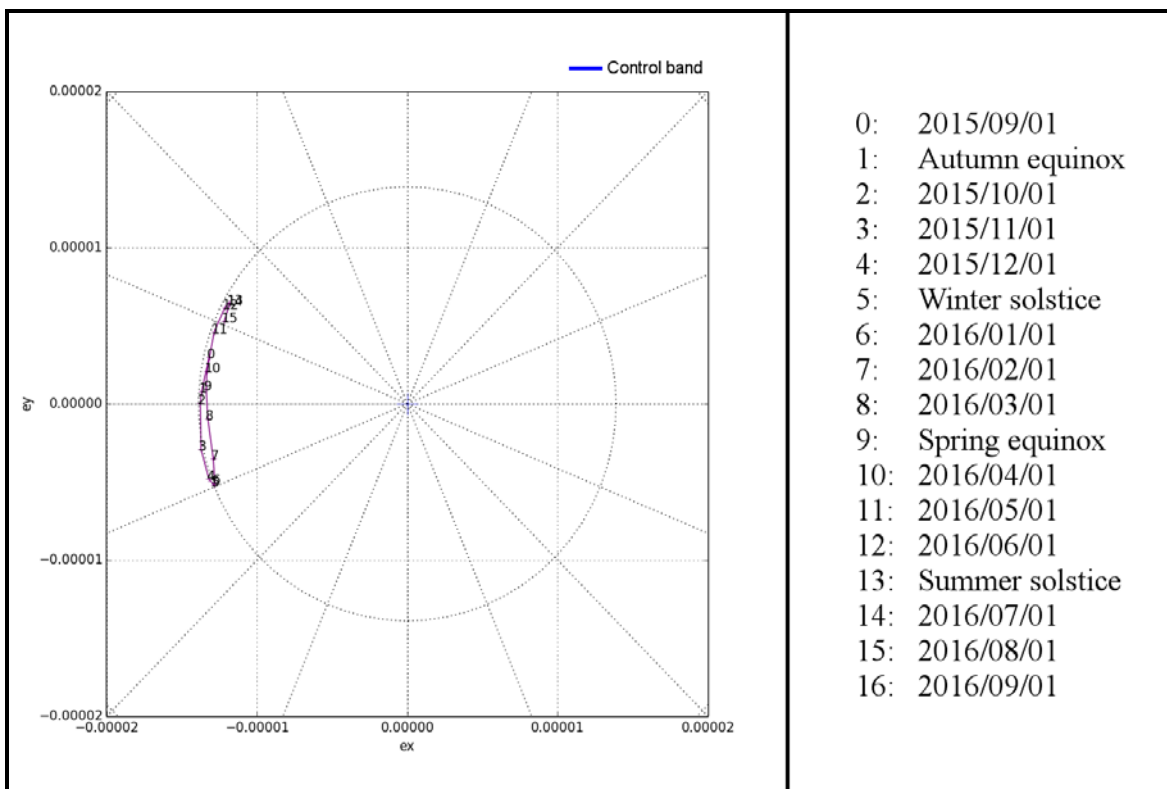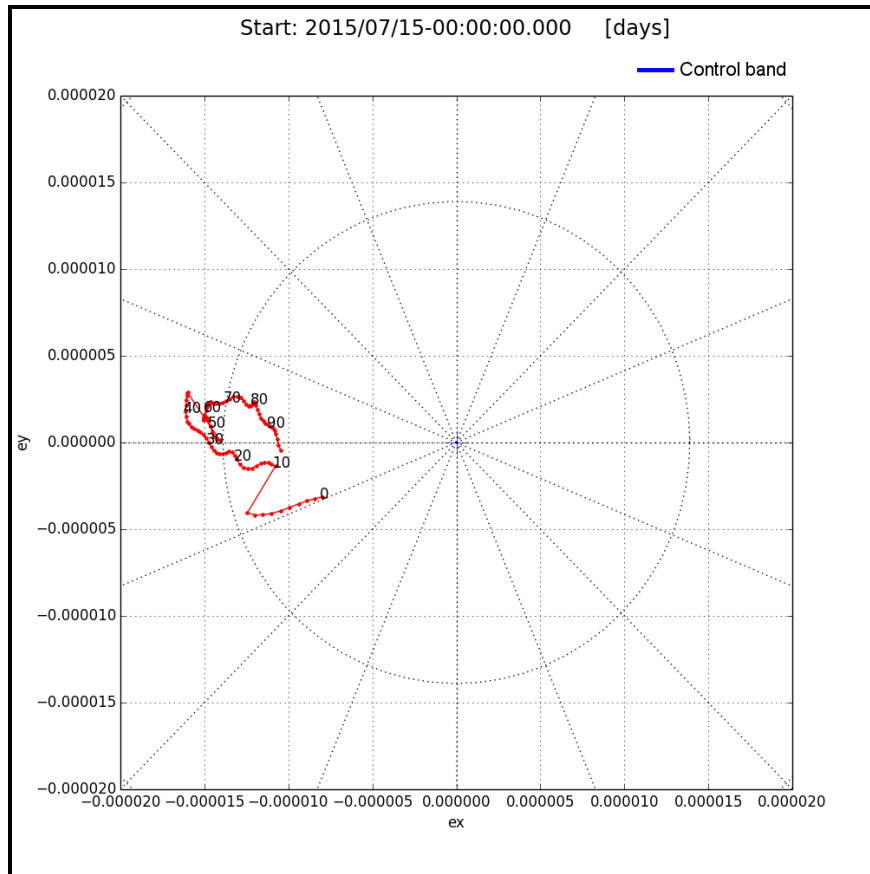| 0: | 2015/09/01 |
1:	Autumn equinox
2:	2015/10/01
3:	2015/11/01
4:	2015/12/01
5:	Winter solstice
6:	2016/01/01
7:	2016/02/01
8:	2016/03/01
9:	Spring equinox
10:	2016/04/01
11:	2016/05/01
12:	2016/06/01
13:	Summer solstice
14:	2016/07/01
15:	2016/08/01
16:	2016/09/01

Figure 8: ICR positions for Sentinel-2

Figure 9: Sentinel-2 eccentricity control in routine

7. References

[1] David A. Vallado. "Fundamentals of Astrodynamics and Applications" ISBN 0-7923-6903-3.

[2] M. Rosengren. "Improved Technique for Pasive Eccentricity Control" American Astronautical Society Publication, AAS-89-155, 1989.

[3] Dennis D. McCarthy (ed.). "IERS Standards (1989). (IERS Technical Note ; 3). Chapter 14: Radiation Pressure Reflectance Model" Paris: Central Bureau of IERS - Observatoire de Paris, 1989. iv, 77 p.

[4] M.A. Martin Serrano, X. Marc, I. Shurmer. "Sentinel-1: operational approach to the orbit control strategy" 23d ISSFD proceedings. Pasadena, USA November 2012.